Rev.Adv.Mater.Sci. 26(2010) 48-57

THE INFLUENCE OF POINT DEFECTS ON THE ELECTRONIC AND MAGNETIC PROPERTIES OF BERYLLIUM MONOXIDE

I.R. Shein[1], M.A. Gorbunova[2], V.S. Kiiko[2] and A.L. Ivanovskii[1]

[1]Institute of Solid State Chemistry, Ural Branch of the Russian Academy of Sciences, 620990, Ekaterinburg, Russia
[2]Ural State Technical University, Ekaterinburg, 620001, Russia

Received: March 02, 2010

Abstract. Owing to unusual thermal, mechanical, electronic and transport properties, beryllium monoxide BeO belongs to the most technically promising ceramic materials for electronic, nuclear, aerospace, electrotechnical, and other advanced applications.
A lot of interesting physical properties of metal-oxide systems, which are not characteristic of the pure compounds, may arise in the same materials containing impurities or other point defects. Computational *ab initio* theory is an effective approach in the determination of structural, magnetic, optical, dielectric and superconducting properties of materials, as it involves no *a priori* assumptions about the electronic structure and atomic interactions, and creates new opportunities for design of new materials with promising properties.
This review focuses on the results of systematic *ab initio* simulations of the influence of point defects (s, p, d impurities, as well as anionic and cationic lattice vacancies) on the electronic and magnetic properties of BeO. The new effects such as impurity-induced magnetism, vacancy-induced magnetism and mixed (impurity+vacancy)-induced magnetism of BeO are discussed in detail. Finally, the theoretical models of predicted BeO nanotubes and the influence of point defects on their properties are considered.

1. INTRODUCTION

Beryllium oxide (BeO) possesses many unique properties such as hardness, a wide energy gap, high transparency over a wide spectral range, considerable efficiency of conversion and accumulation of the energy of ionizing radiations, as well as high radiation resistance, chemical durability, and thermal stability, and therefore has great potential for electronic, nuclear, aerospace, electrotechnical, and other advanced applications. This generated much interest in synthesis, physical properties, and computer simulation of beryllium oxide and related materials, see [1,2].

A very important problem for BeO is the presence of various intrinsic point defects (first of all - lattice vacancies and interstitial impurities) and their effect on the properties of this material. Numerous experimental studies demonstrated strong influence of these defects on the anomalies in various properties of BeO samples. In turn, the introduction of point defects is an effective approach to optimizing the properties of BeO ceramics for various applications – for example, for scintillation detectors and thermoluminescence and exoelectron dosimeters for ionizing radiation *etc*. [1-9].

Besides experimental efforts, a lot of interesting results about the physical properties of beryllium-oxide systems with various defects were obtained recently using computational *ab initio* theory, which is an effective way to determine structural, mag-

Corresponding author: A.L. Ivanovskii, email: ivanovskii@ihim.uran.ru

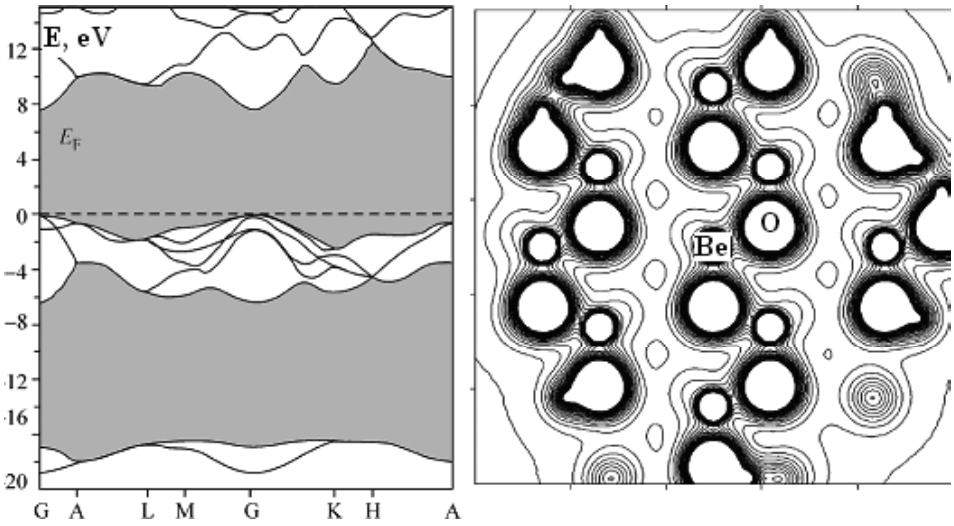

Fig. 1. Band structure and electronic density distribution for BeO.

netic, optical, dielectric and superconducting properties of materials, as it involves no *a priori* assumptions about the electronic structure and atomic interactions, and creates new opportunities for design of new materials with promising properties.

This review focuses on computer simulation studies of the electronic and magnetic properties of BeO with various point defects, namely s, p, d *interstitial* impurities, as well as anionic and cationic lattice vacancies. The new effects such as impurity-induced magnetism, vacancy-induced magnetism and mixed (impurity+vacancy)-induced magnetism of BeO are discussed in detail. Finally, the theoretical models of predicted BeO nanotubes and the influence of point defects on their properties are considered.

2. ELECTRONIC PROPERTIES OF BULK BeO

BeO crystallizes in the hexagonal wurtzite-like structure with the space group *P*63*mc* and with the Be atoms in positions (0, 0, 0) and (1/3, 2/3, 1/2), and the oxygen atoms in (0, 0, *z*) and (1/3, 2/3, 1/2+*z*). Therefore, the structure of BeO is defined by its lattice parameters (*a* and *c*) and the positional parameter *z* [1,2] The band structure of BeO was studied using a variety of approaches based on the density-functional theory (DFT) [2,10-17]. The valence spectrum of BeO, ~18.7 eV in width, comprises two groups of energy bands separated by gap at about 9.9 eV, Fig. 1. The lower bands are derived from O 2*s* states, and the upper bands - from O 2p states.

According to different DFT calculations, the forbidden band gap between the valence and conduction bands (direct transition at point Ã) is about 7.4 eV, which is substantially smaller than the measured band gap (10.6 eV [1,2]). Band gap underestimation (by 30–50%) for dielectrics is a well-known feature of LDA-based methods [18,19]. A standard correction procedure is to introduce an empirical coefficient, K_e, which is typically 1.4–1.6 for oxide phases [18]. Based on the DFT results, K_e for BeO is estimated to be ~1.45.

Band structure results can be used to analyze chemical bonding in BeO. Fig. 1 shows the charge density map along the Be–O bond and in the BeO crystal [16]. The wave functions of the Be and O ions are seen to partially overlap, indicating that the Be–O bond is partly covalent. According to Ref. [10], the effective atomic charges are $Q^{Be} = 1.75e$ and $Q^{O} = 6.24e$; the bond $\{Q^{O}/\{Q^{O} + Q^{Be}\}$ is by about 56% of fractional ionic character.

Let us note that band structure calculations were used to determine the effective electron mass, to study optical properties, spontaneous polarization, piezoelectric constants, elastic properties for BeO and some other compounds, see review [9].

3. LATTICE VACANCIES

Experimental evidences of the presence of lattice vacancies in crystalline wurtzite-like beryllium oxide have been reported in monograph [2].

The problem of the influence of beryllium vacancies V_{Be} (as well as beryllium interstitials Be_i and the defect $\{V_{Be} + Be_i\}$) on the electronic compositions $BO_{0.972}X_{0.0}$ properties of BeO was studied for the first time in [20]. The most stable configurations

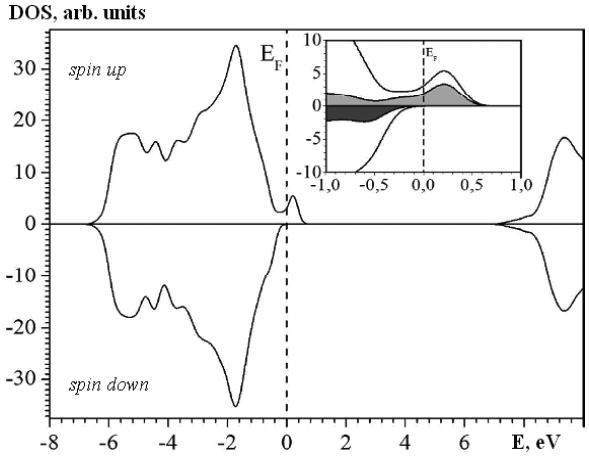

Fig. 2. Spin-resolved densities of states for oxygen-deficient $Be_{1-x}O$. *Insert*: the contributions to the total DOS of $Be_{0.972}O$ from the O2$p\uparrow$ and O2$p\downarrow$ states of the oxygen atoms surrounding the Be vacancy near the Fermi level.

of defects among those considered are vacancies and interstitial Be atoms occupying octahedral positions at R ~3.15-3.35 Å distances from each other. It was also found that depending on the configuration of defects, the forbidden gap of beryllium oxide can change by ~0.4-2.4 eV.

More detailed investigations of the influence of cationic and anionic lattice defects on the electronic and magnetic properties of BeO lead to very unexpected results [21,22]. The supercell approach was employed, where pure BeO was described by the 72-atomic supercell $Be_{36}O_{36}$. Further, the supercells $Be_{35}O_{36}$ and $Be_{36}O_{35}$ simulate the non-stoichiometric compositions $Be_{0.972}O$ and $BeO_{0.972}$, respectively. The results show that the ground state of the ideal BeO is nonmagnetic.

The main finding for non-stoichiometric $Be_{0.972}O$ and $BeO_{0.972}$ [21,22] is that creation of vacancies in Be or O sublattices of BeO may result in quite different effects. Namely, the presence of oxygen vacancies leads to a metallic-like type spectrum for non-stoichiometric compositions $Be_{1-x}O$, but the initial non-magnetic state of the matrix is preserved. On the contrary, for $Be_{0.972}O$ the beryllium vacancy behaves as a *p*-type dopant; as a result, the Fermi level moves to the valence band top, and the non-stoichiometric $Be_{0.972}O$ becomes also metallic, Fig. 2. Besides, the partially occupied O 2*p* band adopts spin splitting, *i.e.* for the spin-down-channel the DOS at the Fermi level $N\uparrow(E_F) > 0$, whereas the spin-up-channel preserves a gap, *i.e.* $N\downarrow(E_F) = 0$.

As is known, such types of spectra are typical of the so-called *magnetic half-metals* (MHM) [23-

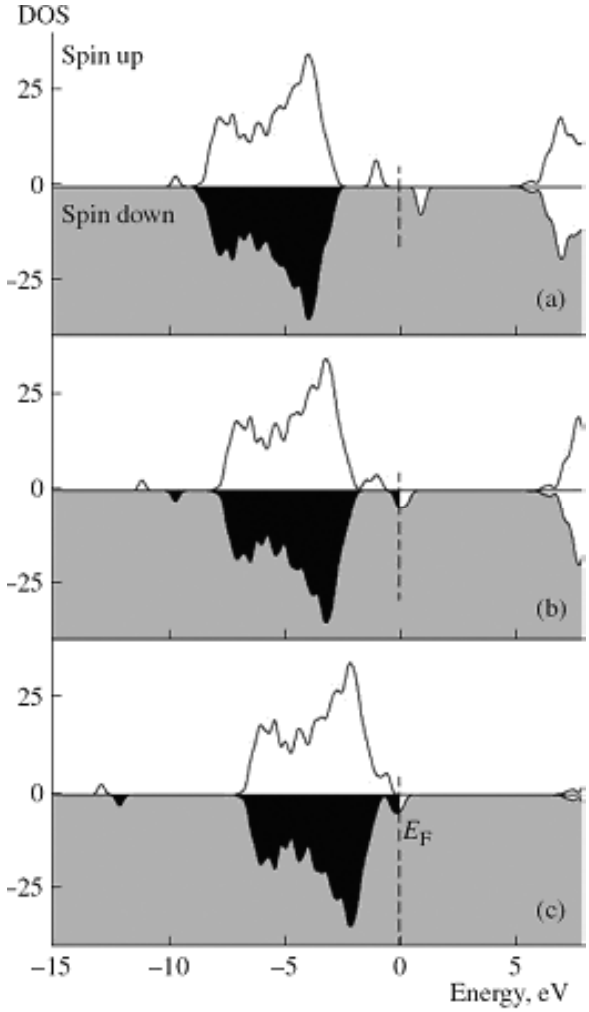

Fig. 3. Spin-resolved DOSs for doped BeO: (a) BeO:B, (b) BeO:C and (c) BeO:N ($E_F = 0$).

26]. These systems are characterized by nonzero density of carriers at the Fermi level (E_F) for one spin projection ($N\downarrow(E_F) > 0$), but they have a forbidden gap (FG) for the reverse spin projection ($N\uparrow(E_F) = 0$). Therefore, in the ideal case for MHMs, spin density polarization at the Fermi level is $P = \{N\downarrow(E_F) - N\uparrow(E_F)\}/\{N\downarrow(E_F) + N\uparrow(E_F)\} = 1$. As a result, conduction in magnetic half-metals occurs along preferred spin channels, and MHM materials exhibit nontrivial spin-dependent transport properties.

Note that the magnetization of $Be_{0.972}O$ is determined by spin-splitting of O2$p\downarrow\uparrow$ bands nearest to V_{Be}. The magnetic moments on the O atoms close to the Be vacancy are about 0.29÷0.40 μ_B, whereas no noticeable magnetic moments are found for the other atoms located at larger distances from the vacancy. Thus, oxygen-deficient $Be_{1-x}O$ demonstrates the novel effect of *vacancy-induced magnetization* of oxide lattice atoms.

4. IMPUTRITIES OF SP ELEMENTS

Recently, the electronic and magnetic states of a nonmagnetic insulator - beryllium oxide doped with nonmagnetic 2*p* elements (boron, carbon, and nitrogen) were studied using the DFT theory [22,27]. The most interesting conclusion followed from computational analysis of the magnetic behavior of boron, carbon, and nitrogen impurities in BeO (for the systems with formal $_{28}$, X = B, C, N) is that the spectrum of doped BO:X systems is typical of the above mentioned magnetic half-metals.

Indeed, for $BeO_{0.972}C_{0.028}$, the introduction of carbon impurity C (into oxygen position) leads to the appearance of a new impurity 2*p* band localized in the band gap of the matrix [27]. The Fermi level is shifted and moves in the region of this 2*p*-like impurity band. The impurity band splits into two spin-resolved C 2*p*↓↑ bands so that the C 2*p*↑ band becomes fully occupied, whereas the C 2*p*↓ band is partially occupied, see Fig. 3. As a result, the insulating BeO becomes a magnetic half-metal.

Let us note that in the doped BeO:C system, the 2*p* states of the impurity center undergo the maximum spin splitting, whereas the induced magnetic moments (MMs) of the matrix atoms closest to the impurity, *i.e.* beryllium and oxygen atoms (because of hybridization of C2*p*-Be2*s*,2*p*, O2*p* orbitals), are much smaller: about 0.08 μ_B and 0.06 μ_B, respectively, *cf.* the MM on carbon is about 0.75 μ_B. The complete picture of magnetization of the BeO:C system may be illustrated using the map of differential spin density $\Delta\rho\downarrow\uparrow = r\downarrow - r\uparrow$, Fig. 4. It should be noted that the contours of $\Delta\rho\downarrow\uparrow$ are considerably deformed in the direction of the interatomic bond lines, which points to the participation of uncompensated spin density in the dopant-matrix bonding.

For related BeO:(B,N) systems, spin splitting of the (2*p*↑ - 2*p*↓) states for boron and nitrogen was found too, Fig. 3. As a result, the following effects occur in the BeO:B → BeO:C → BeO:N series: (i) The BeO:B system undergoes a transition to the semiconducting magnet state, whereas the BeO:C and BeO:N systems become half-metal magnets; at the same time, in the BeO:C BeO:N series, the filling of the X2p↓ band and the value of $N\downarrow(E_F)$ increase; (ii) For the high-spin system, the band gap increases from 5.01 eV (for BeO:B) to 6.27 eV for BeO:N; (iii) The magnetic moments of the doping atoms decrease noticeably from $1.16m_B$ (for BeO:B) to $0.42m_B$ (for BeO:N); the induced magnetic moments at the Be and O atoms and the resulting magnetization of the doped system decrease simultaneously. In summary, BeO:(B,CN) systems exhibit *impurity-induced magnetism*, which is due mainly to dopant centers - in contrast to the above-mentioned *vacancy- induced magnetization* of host atoms in non-stoichiometric beryllium monoxide.

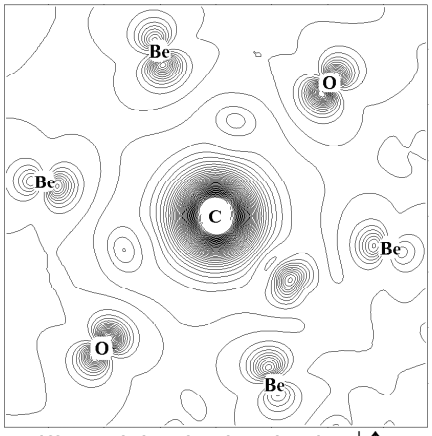

Fig. 4. Differential spin density ($\Delta\rho\downarrow\uparrow = r\downarrow - r\uparrow$) map for the doped BeO:C system.

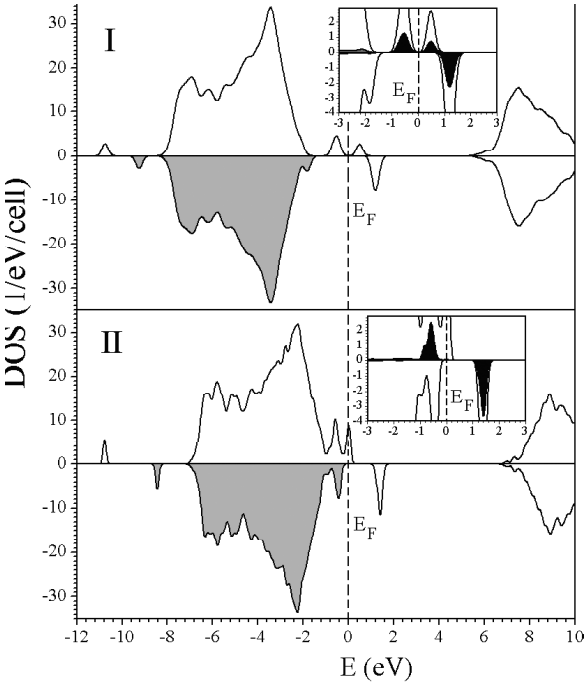

Fig. 5. Spin-resolved total density of states for BeO with the lattice defects $V_{Be} + C_O$ ($Be_{0.972}O_{0.972}C_{0.028}$) which are placed: (I) - far from each other and (II) - in the vicinity to each other. *Insert*: spin-resolved C 2*p*↓↑ DOS for carbon impurity.

5. IMPUTRITIES OF SP ELEMENTS + LATTICE VACANCIES

As is shown above, magnetization of the nonmagnetic BeO can arise both owing to introduction of

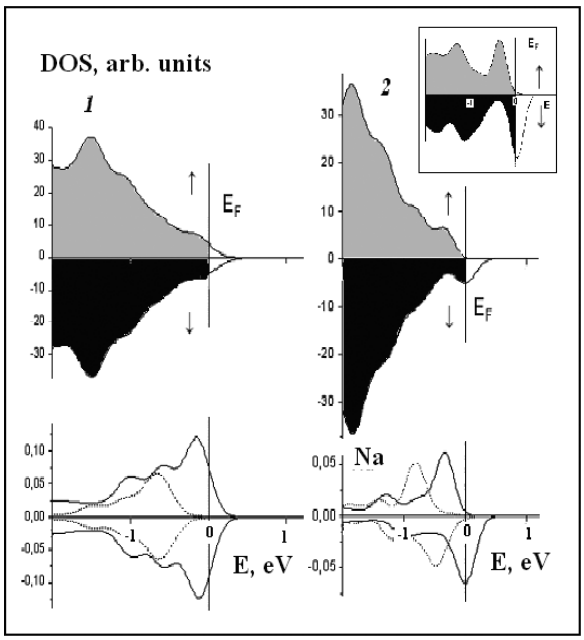

Fig. 6. Total spin-resolved DOSs for BeO doped with Li (1) and Na (2). Below: Spin density σ (dotted line) and s (full lines) states of lithium and sodium impurities. E_F = 0 eV. *Insert:* Spin-resolved oxygen 2p states for BeO:Na.

non-magnetic sp impurities and the presence of lattice vacancies. The joint scenario, *i.e.* simultaneous presence of the beryllium vacancy (V_{Be}) and carbon atom substituting for oxygen (C_O), was examined in [22]. The results (Fig. 5) show that when the impurity and the vacancy are placed at the nearest positions, the system becomes a magnetic half-metal, where the near-Fermi bands are composed by O 2*p*↑ states, and the highest magnetic moment ($1.17\mu_B$) refers to the carbon impurity C_O. However, when the impurity and the vacancy are placed far from each other, the system becomes a magnetic semiconductor with the band gap at about 0.1 eV between the occupied and empty bands of a mixed composition: (O 2*p*↑ + C 2*p*↑).

In this case, the highest magnetic moment ($0.79\mu_B$) also belongs to C_O. Comparison of the total energies (E_{tot}) for $Be_{0.972}O_{0.972}C_{0.028}$ with C_O and V_{Be} placed in various mutual positions shows that the most preferable (ΔE_{tot} ~2.10 eV/cell) arrangement of these defects is in the vicinity of each other, when the system becomes a magnetic half-metal. However, the magnetization of this system (MM($Be_{0.972}O_{0.972}C_{0.028}$) = 1.19 μ_B, per cell) decreases in comparison with BeO in the presence of single defects: beryllium vacancy V_{Be} (MM($Be_{0.972}O$) 1.86μ_B, per cell) or carbon impurity C_O (MM($BeO_{0.972}C_{0.028}$) = 1.52 μ_B, per cell).

6. IMPURITIES OF S METALS

The influence of *s*-atoms (lithium and sodium) on the electronic properties of BeO was examined in [28]. Li impurities produce additional states between two filled bands and in the band gap of BeO. The local levels in the band gap are derived from the Li states and the O2*p* states of the oxygen atoms that coordinate the impurity. The system BeO:Li remains non-magnetic.

Oppositely, for BeO:Na the simulation performed indicates that the non-magnetic insulator BeO is transformed into a magnetic half-metal owing to spin splitting of 2*p* states of oxygen atoms, Fig. 6. Let us note that the situation, in which Na behaves as a *p*-type dopant, is similar to that for the Be-deficient beryllium oxide. The calculated total MM (per cell) for $Be_{0.972}Na_{0.028}O$ is about $0.81\mu_{Å}$.

7. IMPUTRITIES OF D METALS

Recently, the effect of impurities - all transition 3*d* metal ions (Sc, Ti….Cu, Zn) on the electronic and magnetic properties of BeO was systematically studied in [29]. Fig. 7 presents the total density of states (DOS) of $Be_{0.972}M_{0.028}O$ (M = Sc, Ti….Cu, Zn). In $Be_{0.972}Sc_{0.028}O$, because of additional electrons brought by scandium, the Fermi level shifts to the bottom of the conduction band (CB), and the system becomes metallic-like.

Quite a different situation is observed for ternary alloys with other 3*d* impurities, which become magnetic. There are some important peculiarities in the occupation of spin-up and spin-down bands with an increase in the number of *d* electrons as going from Ti to Cu, which determine the changes in the density of states at E_F ($N(E_F)$) and the behavior of local magnetic moments.

From the DOS in Fig. 7 it is seen that for $Be_{0.972}Ti_{0.028}O$ the new Ti3*d*-induced impurity band occurs in the gap (near the bottom of CB), where the Fermi level is within this *d* band for the spin up electrons and within a gap for the spin down electrons. Further modification of $Be_{0.972}M_{0.028}O$ spectra is determined by two factors: the downward shift of impurity M3*d* bands and an increase in their filling owing to the growing number of *d* electrons. For early impurities, the variation of the band filling and $N(E_F)$ is mainly due to the filling of the spin-up band peak, which is moved below E_F as going from Ti to Mn. As a result, these alloys adopt the HMM state,

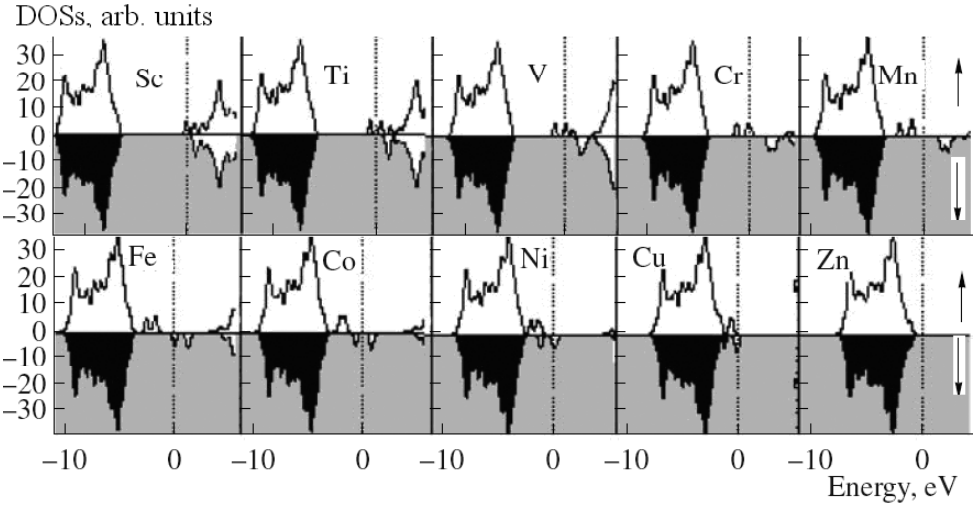

Fig. 7. Spin-resolved total DOSs for $Be_{0.972}M_{0.028}O$ solid solutions, where M are 3d metals.

for which the spin-up-channel is of a metallic-like type, whereas the spin-down-channel preserves a gap at the Fermi level. Note that the splitting of M*d*↑-M*d*↓ bands increases when going from Ti to Mn. A critical limit of this kind of band filling is achieved for $Be_{0.972}Mn_{0.028}O$ alloy where all Mn*d*↑-states are occupied, whereas all Mn*d*↓-states are empty and are separated from Mn*d*↑-states by a gap (~1.89 eV). Thus, in contrast to the earlier mentioned HMM materials, this alloy is a magnetic semiconductor with the maximal MM, Fig. 8.

A different situation is observed for $Be_{0.972}M_{0.028}O$ alloys with the late 3*d* impurities (Fe, Co, Ni, and Cu). As can be seen from Fig. 7, in the Fe-containing alloy all *d*↑ states are filled, whereas the states around the Fermi level are derived mainly from spin-down Fe3*d* orbitals. As going from Fe to Cu, the splitting of *d*↑ - *d*↓ bands decreases simultaneously with filling of *d*↓ bands. Thus, the inversion of spin-channel occupation occurs for these alloys, whose HMM behavior is due to the fully occupied spin-up band (having a band gap at the Fermi level), whereas the contribution to $N(E_F)$ is due to the spin-down impurity states. Finally, for $Be_{0.972}Zn_{0.028}O$ alloy all occupied impurity states are localized inside the BeO valence band, and the system returns to the non-magnetic state.

For all the considered systems, magnetism originates from spin polarization of 3*d* impurities, whereas induced magnetization on the nearest atoms of the matrix (oxygen and beryllium) is very small. For example, for $Be_{0.972}Co_{0.028}O$ alloy the induced moments on oxygen ($0.028\mu_B$) and Be ($0.002\mu_B$) are very small as compared with cobalt ($2.433\ \mu_B$). Figure 8 shows the variation of local magnetic moments

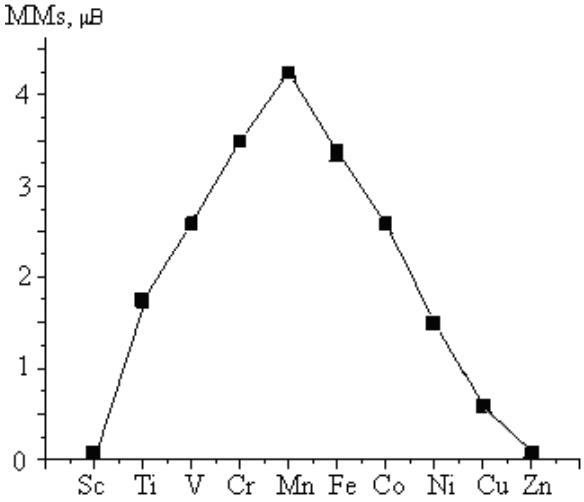

Fig 8. Atomic magnetic moments of impurities across the 3*d* series in $Be_{0.972}M_{0.028}O$ alloys.

of impurities ($LMM^{(i)}$) in $Be_{0.972}M_{0.028}O$ and $Be_{0.944}M_{0.028}O$ alloys for the 3*d* series. As is seen, these dependences are of a nonlinear type.

Thus, it may concluded that addition of 3*d* metal ions into BeO transforms the initial non-magnetic insulating material BeO into various ternary alloys, among which there are nonmagnetic metals, semiconductors, magnetic metals, and half-metals [29].

8. BeO NANOTUBES AND THE INFLUENCE OF POINT DEFECTS ON THEIR PROPERTIES

Very recently, atomic models of pristine beryllium monoxide nanotubes (BeO NTs) were proposed and their structural, cohesion and electronic properties were predicted [30,31]. It was found that these nanotubes are wide-band-gap dielectrics with very

small helicity-induced differences in the gaps [31]. In addition, BeO NTs adopt interesting mechanical properties, namely their Young's moduli are comparable with those for carbon nanotubes [30].

The possibility of improvement of the functional properties of BeO NTs as potential advanced materials and of the magnetization of *non-magnetic* BeO nanotubes by introduction of *non-magnetic sp* impurities, as well as the role of oxygen vacancies in the tube walls are examined in [32].

For this purpose, the pristine infinite-long BeO nanotubes are constructed in a conventional way (see, for example [33-40]) by rolling of BeO graphitic sheets into cylinders. In this way, three groups of BeO-NTs can be created depending on the rolling direction: non-chiral *armchair* (*n*,*n*)-, *zigzag* (*n*,0)- and chiral (*n*,*m*)-like tubes. Two non-chiral nanotubes, namely, *zigzag* (10,0) and *armchair* (6,6) BeO NTs with comparable radii, are examined, Fig. 9. For the simulation of B, C or N doped BeO nanotubes, an oxygen or beryllium atom is removed from the tube wall and replaced by the above *sp* atom. In turn, the removing of beryllium or oxygen atoms simulated the formation of the corresponding wall vacancies; the calculations are performed using the SIESTA code [41].

The results obtained [32] lead to the following conclusions. Firstly, for B, C, and N doped BeO tubes, the geometry optimization does not lead to any dramatic distortion of the initial BeO NTs structure; this means that the doped BeO tubes are stable and their cylinder-like morphology is retained. Secondly, the calculations show [32] that upon replacement of beryllium atom by all the above *sp* impurities these systems still remain non-magnetic (as was predicted also for the crystalline BeO, see above), and therefore they will not be discussed further.

The picture is quite different when *sp* dopants are placed in the oxygen sites, and the doped BeO:(B,C,N) NTs tubes become magnetic. In this case, the total magnetic moments (MM, per cell) in the doped BeO tubes vary from 2 to 1 μ_B. At the same time, the maximal (1.6 - 0.75 μ_B) MMs are localized on the impurity centers, whereas the MMs of the neighboring beryllium (0.12 - 0.01 μ_B) and oxygen (0.06 - 0.01 μ_B) atoms are much smaller.

It is interesting to note that in the sequence of doped nanotubes BeO:B $\rightarrow$ BeO:C $\rightarrow$ BeO:N, the total MMs and magnetic moments of *sp* dopants vary non-monotonically adopting the maximal values for the BeO:C tube. This situation differs drastically from the bulk BeO, when MMs for the crystalline BeO lower in the sequence of dopants B $\rightarrow$ C $\rightarrow$ N. Probably, these differences are caused mainly by the features of electronic distributions of four-fold coordinated atoms in wurtzite-like (type *B*4) beryllium monoxide crystal *versus* three-fold coordination of atoms inside BeO tube walls.

The origin of the mentioned effect may be discussed using the DOSs for the doped BeO:(B,C,N) NTs, Fig. 9. The data presented show that the impurity-induced magnetization for BeO nanotubes originates mainly from spin splitting of *sp* impurity atoms states. As can be seen from the *l*-projected density of states (Fig. 9), the introduction of all the impurities (B, C and N) in the BeO tube walls leads to: (i) occurrence of new impurity 2*p* bands localized in the gap of the BeO NTs; (ii) a shift of the Fermi level (E_F), which is located in the region of these 2*p*-like impurity bands; and (iii) splitting of these impurity bands into two spin-resolved bands with various types of filling. This results in the above magnetization, and non-magnetic BeO tubes become magnetic semiconductors.

The formation of vacancies in Be or O positions of BeO nanotubes gives rise to quite different effects [32]. Namely, for the BeO tubes with oxygen vacancies no spin polarization effects occur and the initial non-magnetic state of the ideal BeO tubes is preserved. On the contrary, for beryllium-deficient BeO NTs the O 2*p* band adopts spin splitting. As a result, magnetization of beryllium-deficient tubes is determined by spin-splitting of $2p\downarrow\uparrow$ bands of oxygen atoms nearest to the beryllium vacancy, and the magnetic moments on the O atoms close to the Be vacancy are about 0.7 - 0.6 μ_B, whereas no noticeable magnetic moments are found for the other atoms located at larger distances from the vacancy. Note that for the $Be_{1-x}O$ NT there is an unoccupied peak in the $2p\downarrow$ spin states above the Fermi level (*i.e.* DOS at the Fermi level $N\downarrow(E_F) > 0$), while the majority of spin channels remain semiconducting, and $N\uparrow(E_F) = 0$. As a result, beryllium-deficient tubes behave as magnetic half-metals.

Thus, the electronic and magnetic characteristics of BeO NTs (such as magnetic moments and band gaps) will depend strongly on the type of the impurities or wall vacancies (and, evidently, on their concentration) and on their positions, and therefore it can be controlled. Namely, if beryllium atoms are replaced by the above *sp* impurities, or oxygen vacancies are present in the tube walls, the BeO NT systems remain non-magnetic.

On the contrary, when *sp* dopants are placed in oxygen sites, or in the presence of beryllium vacan-

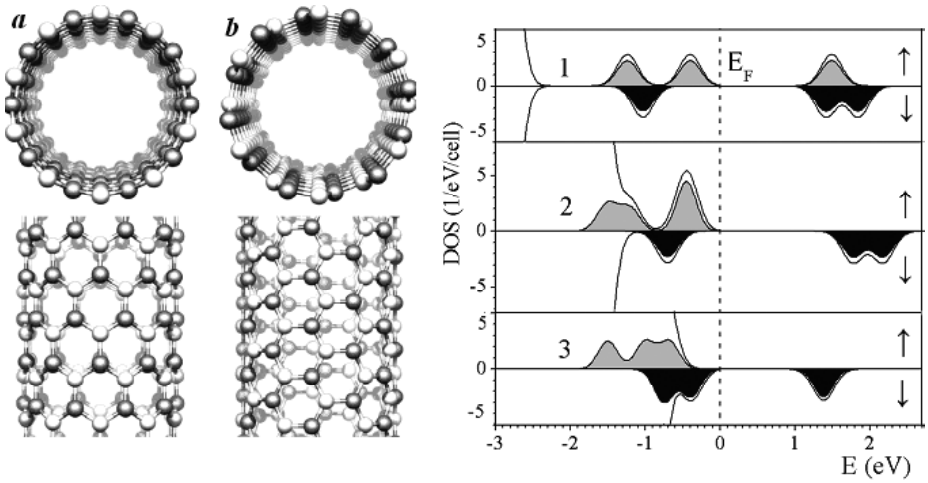

Fig. 9. (*Left*) Top and side views of atomic structures of single-walled: *a*.- *zigzag* (10,0) and *b*- *armchair* (6,6) nanotubes of graphite-like hexagonal BeO. (*Right*) Majority and minority total spin densities of states for boron (1), carbon (2) and nitrogen-doped (3) *armchair* (6,6) BeO nanotube (*full lines*) and B, C and N impurity atoms $2p\downarrow\uparrow$ states (*shaded*). The Fermi level is given at 0.0 eV.

cies, the effects of the so-called *sp-impurity-induced magnetism* or *vacancy-induced magnetism*, respectively, are found.

The results [32] confirm that the systems, which contain no magnetic transition-metal atoms, undergo a transformation from non-magnetic insulators (pristine BeO nanotubes) to magnetic semiconductors or magnetic half-metals. It is found that the magnetization mechanism for these systems is essentially different and should be attributed to (i) spin splitting of (B,C,N) $2p\downarrow\uparrow$ bands for *sp* doped BeO NTs, whereas magnetization of Be and O atoms is relatively small, and (ii) spin-splitting of $2p\downarrow\uparrow$ bands of "intrinsic" oxygen atoms - for beryllium-deficient BeO NTs. Moreover, the band gaps for *sp*-doped BeO NTs are determined by impurity spin-polarized bands and decrease drastically as compared with pristine BeO tubes - from 5.9 eV to 1.0-1.5 eV. At the same time, these beryllium-deficient tubes behave as magnetic half-metals.

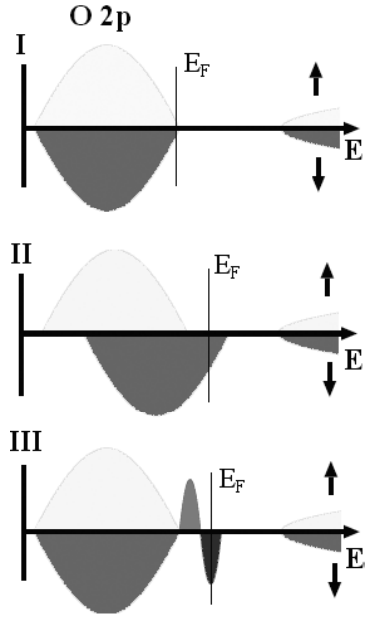

Fig. 10. Models of the electronic spectra of: I. Ideal BeO; II. Non-stoichiometric or s-metal-doped BeO (effects of magnetization of oxygen atoms of the matrix) and III. BeO doped with 2p non-metals (B,C,N) or some 3d metals (effects of magnetization of impurity atoms).

9. CONCLUSIONS

In this review, the results of systematic *ab initio* simulations of the influence of point defects (s, p, d impurities, anionic and cationic lattice vacancies) on the electronic and magnetic properties of BeO are discussed. New effects such as impurity-induced magnetism, vacancy-induced magnetism and mixed (impurity+vacancy)-induced magnetism for crystalline BeO and BeO nano-sized structures (nanotubes) are predicted.

Based on the discussed results, a common model may be proposed (Fig. 10). Two main scenarios can arise owing to introduction of point defects into the BeO matrix.

In the first scenario, the Be or O atom is replaced by an atom of smaller valency (or by a vacancy), thus depriving the valence band of an electron. This hole-like doping can shift the Fermi level

into the valence band, and spontaneous spin polarization of 2p states of oxygen atoms of BeO may take place, see Fig. 10, II. Such a mechanism was established for alkali-atom-doped or Be-deficient BeO.

The second scenario is replacement by an atom of higher valency. Such an impurity introduces additional states in the gap of the matrix, and these states may be inclined to spontaneous spin-splitting, see Fig. 10, III.

In conclusion, the present discussion is focused only on the point defects in the BeO matrix, whereas numerous issues for future studies could be proposed. For instance, the influence of impurity and (or) lattice vacancies content variation on the properties of such BeO-based materials is of interest. Further investigations are necessary to compare the energies of ferromagnetic and antiferromagnetic ground states and the exchange interaction magnitudes for estimations of the ferromagnetic critical temperature. The latter studies are significant, in particular, for the application of magnetic half-metallic alloys as DMS-materials for spintronic devices. Research into the joint effect - (impurity+vacancy) - induced magnetization would be of great importance for the understanding of possible ways of controlled changes of magnetic properties of BeO nanomaterials - not only for the considered nanotubes, but also for BeO nano-crystallites, fullerene-like cages [42], as well as for BeO thin films. We believe that the *ab initio* computational methods will be effective for the solution of these problems.

ACKNOWLEDGEMENTS

Financial support from the RFBR (Grants 08-08-00178-a and 10-03-96004-p-URAL-a) is gratefully acknowledged.

REFERENCES

[1] R. A. Belyaev, *Beryllium Oxide* (Atomizdat, Moscow, 1980), in Russian.
[2] V. S. Kiiko, Yu. N. Makurin and A.L. Ivanovskii, *BeO - based ceramics: preparation, physico-chemical properties and application* (Ural Branch of the Russian Academy of Sciences, Ekaterinburg, 2007), in Russian.
[3] V. S. Kiiko, Yu. N. Makurin, A. I. Dmitriev, A. A. Sofronov and A. L. Ivanovskii // *Glass Ceramics* **58** (2001) 419.
[4] V. S. Kiiko, A. A. Sofronov, Yu. N. Makurin and A. L. Ivanovskii // *Glass Ceramics* **60** (2003) 120.
[5] V. S. Kiiko, A. I. Dmitriev, Yu. N. Makurin, A. A. Sofronov and A. L. Ivanovskii // *Glass Phys. Chem.* **30** (2004) 109.
[6] V. S. Kiiko, Y. I. Komolikov, Yu. N. Makurin, I. R. Shein and A. L. Ivanovskii // *Inorg. Mater.* **43** (2007) 1361.
[7] Yu. N. Makurin, M. A. Gorbunova, V. S. Kiiko, I. R. Shein and A. L. Ivanovskii // *Glass Ceramics* **64** (2007) 439.
[8] V. S. Kiiko, M. A. Gorbunova, Yu. N. Makurin, A. D. Neuimin and A. L. Ivanovskii // *Refractor. Indust. Ceram.* **48** (2007) 429.
[9] A. L. Ivanovskii, I. R. Shein, Yu. N. Makurin, V. S. Kiiko and M. A. Gorbunova // *Inorg. Mater.* **45** (2009) 223.
[10]. Y. N. Xu and W. Y. Ching // *Phys. Rev.* B **48** (1993) 4335.
[11]. A. Lichanot, M. Chaillet and M. Larrieu // *Chem. Phys.* **164** (1992) 383.
[12]. W. Lambrecht and B. Segall // *J. Mater. Res.* **7** (1992) 696.
[13]. B. E. Kulyabin, V. A. Lobach and A. V. Kruzalov // *Fiz. Tverdogo Tela* **32** (1990) 3685.
[14]. P. E. Van Camp and V. J. Van Doren // *J. Phys.: Condens. Matter* **8** (1996) 3385.
[15]. V. Milman and M. C. Warren // *J. Phys.: Condens. Matter* **13** (2001) 241.
[16] Yu. N. Makurin, A. A. Sofronov, V. S. Kijko, Y. V. Emelyanova and A. L. Ivanovskii // *J. Structural Chem.* **43** (2002) 515.
[17] I. R. Shein, V. S. Kijko, Yu. N. Makurin, M. A. Gorbunova and A. L. Ivanovskii // *Phys. Solid State* **49** (1007) 1067.
[18] J. Robertson, K. Xiong and S. Clark // *Thin Solid Films* **496** (2006) 1.
[19] P. W. Peacock and J. Robertson // *J. Appl. Phys*. **92** (2002) 4712.
[20] A. A. Sofronov, M. A. Gorbunova, Yu. N. Makurin, V. S. Kiiko and A. L. Ivanovskii // *J. Structural Chem.* **47** (2006) 760.
[21] I. R. Shein and A. L. Ivanovskii // *J. Structural Chem.* **48** (2007) 1145.
[22] I. R. Shein, M. A. Gorbuniva, Yu. N. Makurin V. S. Kiiko and A. L. Ivanovskii // *Intern. J. Modern Phys*. B **22** (2008) 4987.
[23] H. Katayama-Yoshida, K. Sato, T. Fukushima, M. Toyoda, H. Kizaki, V. A. Dinh and P.H. Dederichs // *phys. stat. sol.* (a) **204** (2007) 15.
[24] A. L. Ivanovskii // *Physics - Uspekhi* **50** (2007) 1031.

[25] I. R. Shein, V. L. Kozhevnikov and A. L. Ivanovskii // *JEPT Lett.* **82** (2005) 220.
[26] I. R. Shein, V. L. Kozhevnikov and A. L. Ivanovskii // *Semiconductors* **40** (2006) 1295**.**
[27] I. R. Shein, M. V. Ryzhkov, M. A. Gorbunova, Yu. N. Makurin and A. L. Ivanovskii // *JETP Lett.* **85** (2007) 246.
[28] A.A. Sofronov, A. N. Enyashin, V.S. Kiiko, Yu. N. Makurin and A. L. Ivanovskii // *Issled. Ross* (2003) pp. 1693–1700, http://zhurnal. ape. relarn. ru /articles/2003/142.pdf.
[29] M.A. Gorbunova, I.R. Shein, Yu.N. Makurin, V.S. Kiiko and A.L. Ivanovskii // *Physica B* **400** (2007) 47.
[30] P.B. Sorokin, A.S. Fedorov and L.A. Chernozatonskii // *Phys. Solid State* **48** (2006) 398.
[31] B. Baumeier, P. Krüger and J. Pollmann // *Phys. Rev. B* **76** (2007) 085407.
[32] M.A. Gorbunova, I.R. Shein, Yu.N. Makurin, V.V. Ivanovskaya, V.S. Kijko and A.L. Ivanovskii // *Physica* E **41** (2008) 164.
[33] A.N. Enyashin, Yu.N. Makurin and A.L. Ivanovskii // *Chem. Phys. Lett.* **387** (2004) 85.
[34] A.N. Enyashin, Yu.N. Makurin and A.L. Ivanovskii // *Carbon* **42** (2004) 2081.
[35] A.N. Enyashin, V.V. Ivanovskaya, Yu.N. Makurin and A.L. Ivanovskii // *Phys. Lett. A* **326** (2004) 152.
[36] A.N. Enyashin, V.V. Ivanovskaya, Yu.N. Makurin, V.L. Volkov and A.L. Ivanovskii // Chem. *Phys. Lett.* **392** (2004) 555.
[37] V.V. Ivanovskaya, T. Heine, S. Gemming and G. Seifert // *Phys. Stat. Sol.* b **243** (2006) 1757.
[38] V.V. Ivanovskaya, Ch. Köhler and G. Seifert // *Phys. Rev. B* **75** (2007) 075410.
[39] A.N. Enyashin and A.L. Ivanovskii // Mater. Lett. **62** (2008) 662.
[40] A.N. Enyashin and A.L. Ivanovskii // *Physica E* **41** (2008) 320.
[41] J.M. Soler, E. Artacho, J.D. Gale, A. Garcia, J. Junquera, P. Ordejon and D. Sanchez-Portal // *J. Phys.: Condens. Matter* **14** (2002) 2745.
[42] A.N. Enyashin, Yu. N. Makurin, A.A. Sofronov, V.S. Kiiko, V. V. Ivanovskaya and A. L. Ivanovskii // *Russ. J. Inorgan. Chem.* **49** (2004) 893.